Enhanced Time-Invariant Linear Model for the EMI Prediction of Switching Circuits

Enhanced Time-Invariant Linear Model for the EMI Prediction of Switching Circuits

Riccardo Trinchero, *Member, IEEE,* Igor S. Stievano, *Senior Member, IEEE,* Flavio G. Canavero, *Fellow, IEEE*

***Abstract*—This paper presents an innovative technique for the black-box modeling of the conductive emissions of switching circuits from external observations. The proposed methodology relies on the robust and elegant theory of periodically switched linear systems, providing the user with a tool for the generation of frequency-domain augmented linear time-invariant equivalents. The obtained models offer both a remarkable accuracy for different supply conditions and a deep understanding of the inherent switching mechanisms of this class of devices. The proposed framework also enables the derivation of a simplified enhanced Norton representation which outperforms the classical state-of-the-art models based on linear time-invariant approximations. Model parameters are computed via a blind procedure based on two measurements, only. The feasibility and strength of the proposed approach are demonstrated on a dc-dc boost power converter and on a dc electrical motor via the prediction of their conducted disturbances.**

***Index Terms*—Modeling, frequency domain analysis, switched circuits, power converter, DC motors, electromagnetic conductive interferences, harmonic analysis.**

I. Introduction

In the past Years, many efforts have been spent to propose effective solutions aimed at modeling and characterizing the electromagnetic-interference (EMI) generated by switching circuits. Without loss of generality, switched mode power converters, dc motors and inverters are typical examples belonging to the above classification, since they are inherently characterized by a periodically time-varying behavior arising from the internal activity of the switching components. The above feature unavoidably leads to discontinuous absorbed currents that behave as EMI feeding the power distribution network. To this aim, it is important to devise a modeling strategy which allows to accurately predict the conducted emissions (CE) of a switching device for different filtering schemes and supply configurations [1].

The approaches available in the literature can be classified in terms of the so-called physical- or behavioral-based methods. For the former one, the CE prediction is achieved via the time-domain simulation of a detailed description of a switching circuit by applying the Fourier transform to its steady-state noisy current responses [2]–[5]. In spite of its simplicity, this approach has a number of weaknesses, mainly: (i) it requires an intimate knowledge of the device structure and switching mechanism, and (ii) long time-domain numerical simulations are in general needed in order to guarantee that the variables of the circuit have reached their steady-state. In order to overcome the latter issue, in the last decades a number of alternative ad-hoc techniques for the steady-state analysis of switching circuits have been proposed [6]–[17]. They are however based on a complex mathematical formulation and cumbersome technical solutions, thus restraining their effectiveness for CE prediction.

On the other hand, the typical behavioral-based models developed for the CE characterization of a switching circuit are inspired by the simplified linear time-invariant (LTI) Norton- or Thevenin-like structures in which model parameters are defined in frequency-domain. The key advantage of this class of approaches relies on a blind modeling procedure that does not require any information of the internal structure of devices. In addition, operating in frequency-domain has the inherent strength of readily incorporating in the circuit analysis elements such as lossy transmission lines or devices represented by rational functions approximations or measured parameters [18]. The main drawback of the above models is related to the simplifications which are unavoidably introduced to suppress the time-varying nature of devices (e.g., see [19]–[26] and references therein). Similar to what is known for the case of linearized small-signal models of nonlinear systems, the aforementioned LTI approximations lack of accurately predicting the behavior of a switching circuit for different supply configurations other than the one used for model estimation (e.g., when a filter is interposed between the supply main and the converter or motor). The above two classes of approaches are weakly related to each other, thus providing complementary and partial solutions with opposite features, i.e., they are either simple and coarse or cumbersome and precise.

The aim of this paper is to propose a unified picture that attempts covering the gap between physics- and behavioral-based methods. This is achieved via an innovative modeling scheme for the frequency-domain characterization of switching circuits from external observations. This approach relies on the theory of periodical linear time varying (PLTV) systems [6] and on an augmented representation of the i-v behavior of the input port of a generic switching circuit. This alternative frequency-domain interpretation turns out to be the natural extension of the classical admittance concept used for the LTI case and suggests a further simplification where an enhanced Norton model can be formally derived.

The remaining of the paper is organized as follows. Section II briefly introduces the statement of the problem. Section III summarizes the essential background of PLTV systems supporting the derivation of a compact frequency-domain

R. Trinchero, I. S. Stievano and F. G. Canavero are with the EMC Group, Department of Electronics and Telecommunications, Politecnico di Torino, 10129 Torino, Italy (e-mail: riccardo.trinchero@polito.it, igor.stievano@polito.it, flavio.canavero@polito.it).

augmented representation of a generic switching element which can be easily estimated from external observations. Section IV collects useful remarks justifying the proposed augmented formulation and discusses the effects of its different constitutive parts on the CE prediction. Section V presents, for the first time, an enhanced Norton equivalent that features an excellent trade-off between accuracy and modeling simplicity. Results on the application of the proposed approach to the EMI modeling of a boost converter and of a dc-motor from both simulations and real measurements are collected in Section VI. Final remarks and conclusions are given in Sec. VII.

II. Problem Statement

This Section introduces the illustrative switching circuit depicted in Fig. 1, which will be used hereafter in the paper to discuss the key features of switching circuits and to presents the proposed frequency-domain modeling approach. The switching circuit is considered as a two-terminal PLTV element which behaves as a noisy black-box element fed by the ideal voltage source $e(t)$. The CE of the circuit are fully characterized by the spectrum of the steady-state response of the noisy absorbed current $i(t)$. The objective of this paper is to propose an alternative approach for the behavioral modeling of the CE of a generic switching circuit.

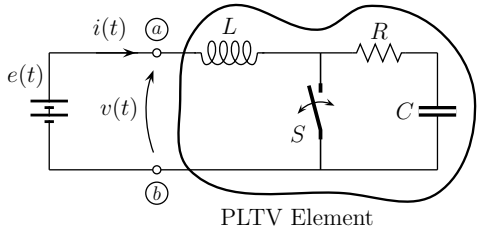

Figure 1: Schematic of the illustrative switching circuit used to present the proposed modeling approaches. The circuit parameters take the following values: $L = 0.1\,\text{mH}$, $C = 0.1\,\text{mF}$, $R = 10\,\Omega$ and the switch S is characterized by a periodic behavior with frequency $f_c = 20\,\text{kHz}$ with duty-cycle $D = 50\%$ and $R_{on} = 1\,\Omega$.

III. Modeling via Augmented Relations

A. Theoretical Background

The discussion starts considering the simplified scenario depicted in Fig. 2 which provides a comparison between the spectra of the current responses $i(t)$ induced on either standard LTI or PLTV elements by a single tone voltage excitation (i.e., a cisoidal excitation at angular frequency Ω).

According to the known fundamental results of linear dynamical circuits, the spectrum of the current response $I(\omega)$ through an LTI element turns out to be a single tone spectra at $\omega = \Omega$, thus allowing the scalar definition of the corresponding admittance $Y_{LTI}(\omega)$ as the ratio between the spectra of the current response and of the voltage excitation. On the other hand, for the case of a PLTV element the spectrum of the current response is characterized by a richer frequency content arising from the coupling between the excitation angular frequency Ω and the switching angular frequency $\omega_c = 2\pi f_c$.

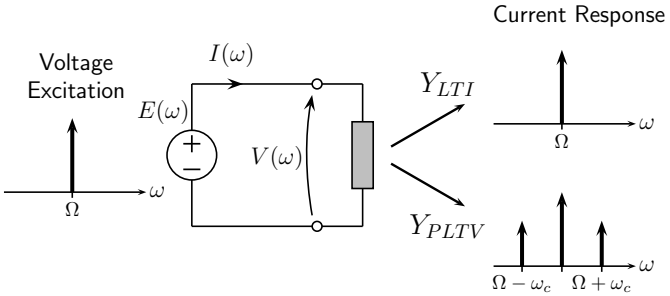

Figure 2: Spectra of the current response $I(\omega)$ of a generic LTI and PLTV element to a single tone cisoidal excitation $e(t) = v(t) = V_0 \exp(j\Omega t)$.

Indeed, its steady-state response can be represented in terms of its Fourier series expansion [7], which writes:

$$i(t;\Omega) = \sum_{n=-\infty}^{+\infty} I_n \exp\left(j(\Omega + n\omega_c)t\right) \tag{1}$$

where I_n are the harmonic coefficients of the current and Ω provides the center angular frequency of the expansion.

Following the above reasoning, the admittance concept developed for the standard LTI elements needs to be generalized to account for the harmonic coupling introduced by the periodic time-varying activity of the switches. To this aim, the so-called *mixed-domain transfer function* is introduced and defined as follows [6]–[16],

$$Y_{PLTV}(t,\Omega) = \sum_{n=-\infty}^{+\infty} Y_n(\Omega)\exp(jn\omega_c t). \tag{2}$$

According to [6], when a single tone voltage excitation, i.e., $e(t) = V_0 \exp(j\Omega t)$, is applied across the PLTV element, the corresponding steady-state current $i(t;\Omega)$ can be computed via the above time-varying admittance operator $Y_{PLTV}(t,\Omega)$ and the *generalized Ohm's law* [12], [13] as follows:

$$\begin{aligned} i(t;\Omega) &= Y_{PLTV}(t,\Omega)V_0\exp(j\Omega t) = \\ &= \sum_{n=-\infty}^{+\infty} Y_n(\Omega)V_0\exp(j(\Omega+n\omega_c)t). \end{aligned} \tag{3}$$

In addition, to account for possible circuit elements placed between the voltage source and the PLTV element, similar to (4), the voltage $v(t)$ at input port of the PLTV element must be replaced by the following Fourier expansion:

$$e(t) \neq v(t;\Omega) = \sum_{n=-\infty}^{+\infty} V_n \exp\left(j(\Omega + n\omega_c)t\right) \tag{4}$$

therefore, according to (3) and thanks to the linearity of the PLTV element, the resulting current $i(t,\Omega)$ writes:

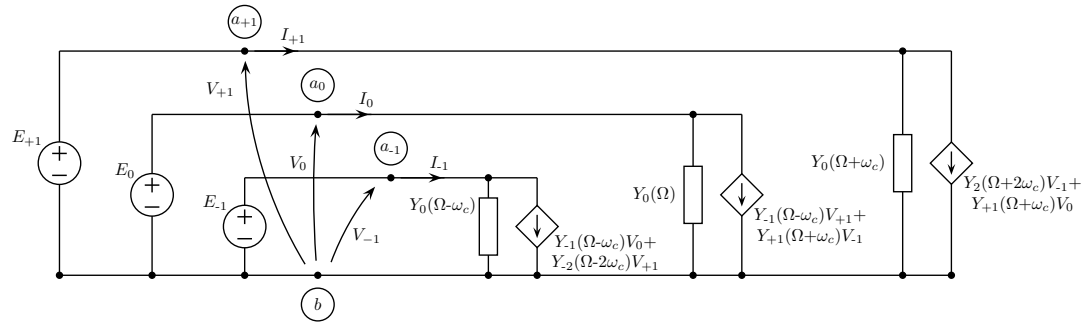

Figure 3: Frequency-domain augmented circuital interpretation of i-v input port behavior of a generic PLTV element (such as the one in Fig. 1) for an expansion order $N = 1$.

$$\begin{aligned}
&\sum_{n=-\infty}^{+\infty} I_n \exp(j(\Omega + n\omega_c)t) = \\
&= \sum_{m=-\infty}^{+\infty} Y_{PLTV}(t, \Omega + m\omega_c) V_m \exp(j(\Omega + m\omega_c)t) \\
&= \sum_{l,m=-\infty}^{+\infty} Y_l(\Omega + m\omega_c) V_m \exp(j(\Omega + (l+m)\omega_c)t).
\end{aligned} \tag{5}$$

For practical reasons, the Fourier expansions from (2) to (5) are conveniently truncated by considering the first $(2N + 1)$ terms, leading the following matrix relation:

$$\mathbf{I} = \mathbf{Y}(\Omega) \cdot \mathbf{V} \tag{6}$$

where $\mathbf{I}$ and $\mathbf{V}$ are vectors of dimension $(2N + 1)$ collecting the harmonic coefficients I_n and V_n of the current and voltage variables through and across the PLTV element, whilst the time-dependent admittance $Y_{PLTV}(t, \Omega)$ is replaced by a square matrix $\mathbf{Y}$ of dimension $(2N + 1) \times (2N + 1)$. As an example, the full expansion of (6) for the case $N = 1$ writes:

$$\underbrace{\begin{bmatrix} I_{-1} \\ I_0 \\ I_{+1} \end{bmatrix}}_{\mathbf{I}} = \underbrace{\begin{bmatrix} Y_0(\Omega - \omega_c) & Y_{-1}(\Omega) & Y_{-2}(\Omega + \omega_c) \\ Y_1(\Omega - \omega_c) & Y_0(\Omega) & Y_{-1}(\Omega + \omega_c) \\ Y_2(\Omega - \omega_c) & Y_1(\Omega) & Y_0(\Omega + \omega_c) \end{bmatrix}}_{\mathbf{Y}(\Omega)} \underbrace{\begin{bmatrix} V_{-1} \\ V_0 \\ V_{+1} \end{bmatrix}}_{\mathbf{V}}. \tag{7}$$

It is important to remark that (6) provides a time-invariant frequency-domain representation of the i-v port behavior of a generic PLTV element, e.g., the one depicted in Fig. 1. Also, the proposed frequency-domain formulation can be considered as the linear interpretation of the harmonic balance technique usually adopted to simulate the steady-state responses in nonlinear circuits [28]. However, in this work the proposed technique will be used for the modeling of the i-v characteristic of a generic PLTV circuit, rather than for simulation purposes only.

B. Circuital Interpretation

The above formulation suggests a frequency-domain circuital interpretation of a switching network in which the harmonics of the voltage and current variables (i.e., V_n and I_n) can be considered as new auxiliary variables in an expanded network that turns out to be $(2N + 1)$ times larger than the original circuit [12]–[16]. For the sake of illustration, Fig. 3 shows the aforementioned augmented network for the case of a generic dynamical PLTV element with an expansion order $N = 1$, for which the characteristic in (7) holds.

The network of Fig. 3 consists of the interconnection of the LTI elements $Y_0(\Omega - n\omega_c)$ corresponding to the diagonal entries of the admittance matrix in (7) and voltage controlled current sources which turn out to be related to the off-diagonal terms. The latter elements are responsible for the coupling among the harmonics of the voltage and current variables at different frequencies. A standard LTI circuit is a special case of the proposed augmented interpretation with $\omega_c = 0$ rad/s for which the admittance matrix $\mathbf{Y}$ turns out to be diagonal and the augmented circuital interpretation collapses into a network without controlled sources. In this simplified picture, the ideal voltage sources on the left represent the voltage excitations arising from the harmonics of the source $e(t)$ in Fig. 1, which is directly connected to the input port of the switching element.

C. Model Estimation & Simulation

Similar to a standard admittance representation of a LTI element, the augmented admittance $\mathbf{Y}(\Omega)$ describing a generic PLTV element centered at Ω can be readily estimated by considering the relationship between the spectra of the currents absorbed by the switching circuit to a predefined set of voltage excitations. Without loss of generality, the simple setup shown in Fig. 4 is considered. It consists of a voltage source $E_k(\omega)$ with its input impedance $Z_{in}(\omega)$ connected to an unknown switching element Y_{PLTV} described by its augmented admittance representation $\mathbf{Y}(\Omega)$ in (7). Knowing the center frequency Ω and the switching angular frequency ω_c, the entries of the unknown augmented admittance $\mathbf{Y}(\Omega)$ can be easily estimated through $(2N+1)$ linearly independent simulations or measurements of the current $I_k(\omega)$ and voltage $V_k(\omega)$ spectra through and across the input port of the PLTV element for a set of voltage excitations $e_k(t) = E_k \cos((\Omega + k\omega_c)t + \phi_k)$ with $k = 0, \ldots, 2N$. The spectrum of the voltage excitations $E_k(\omega)$ is designed to stimulate all the frequency components of the steady-state Fourier expansion in (4).

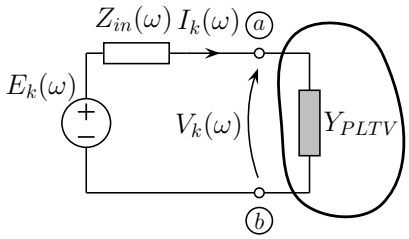

Figure 4: Example circuit used for computing the augmented admittance representation $\mathbf{Y}(\Omega)$ of a generic PLTV element from both simulations or measured data.

According to (6), the spectra of the current and voltage waveforms recorded for $(2N+1)$ measurements can be recasted in term of the following linear system:

$$\mathbf{Y}(\Omega) \approx \begin{bmatrix} | & & | \\ \mathbf{I}_0 & \ldots, & \mathbf{I}_{2N} \\ | & & | \end{bmatrix} \left(\begin{bmatrix} | & & | \\ \mathbf{V}_0 & \ldots, & \mathbf{V}_{2N} \\ | & & | \end{bmatrix} \right)^{-1} \tag{8}$$

where for each mesurements $\mathbf{V}_k$ and $\mathbf{I}_k$ are column vectors containing $(2N+1)$ samples of the current and voltage spectra sampled at $(n\omega_s + \Omega)$ with $n = -N, \ldots, +N$, such that:

$$\mathbf{V}_k = [V_k(-N\omega_s + \Omega), \ldots, V_k(\Omega), \ldots, V_k(N\omega_s + \Omega)]^T, \tag{9}$$

and

$$\mathbf{I}_k = [I_k(-N\omega_s + \Omega), \ldots, I_k(\Omega), \ldots, I_k(N\omega_s + \Omega)]^T. \tag{10}$$

It is important to remark that the proposed modeling scheme turns out to be completely independent from the input impedance of the voltage source $Z_{in}(\omega)$. Also, several measurement technique can be applied with the aim of measuring the voltage $V_k(\omega)$ and the current $I_k(\omega)$ depending on their amplitudes and bandwidth.

A an example, Fig. 5 shows the augmented admittance matrix associated to the input port behavior of the switching circuit in Fig. 1. In this preliminary test, SPICE numerical simulations are used to collect the system responses required to fill the linear system in (8).

Once a generic PLTV circuit element has been characterized via the aforementioned augmented representation, its CE can be easily computed via a well-established simulation procedure as outlined in [13], [14]. However, when the maximum bandwidth of the model $f_{max} = (\Omega + N\omega_c)/2\pi$ is much larger that the switching angular frequency ω_c, the measurement operation becomes unfeasible. This observation motivates the discussion and the simplified modeling approach presented in the next two sections.

IV. Insight into the admittance matrix

This section investigates the effects of the dominant contributions of the augmented matrix on the spectrum of the input port current response of a switching element. Without loss of generality, the following reasoning is based on the admittance

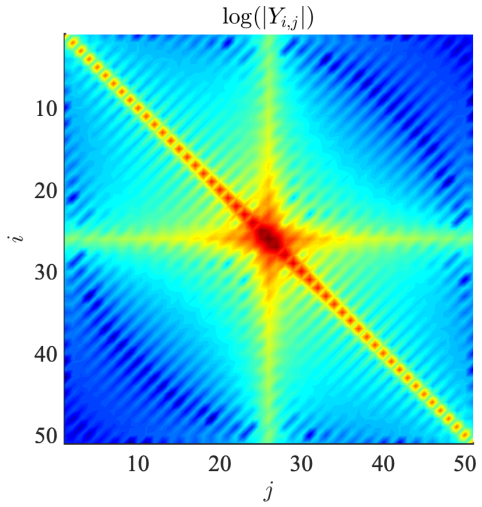

Figure 5: Magnitude of the entries of the augmented admittance $\boldsymbol{Y}$ of the input port of the switching circuit of Fig. 1 for $N = 25$ (red means high magnitude and blue low magnitude).

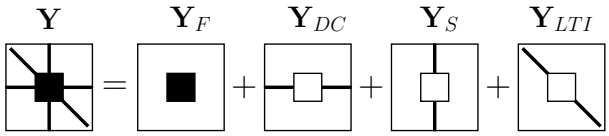

Figure 6: Decomposition of the admittance matrix in terms of its basic constitutive blocks.

matrix $\mathbf{Y}(\Omega = 0)$ of Fig. 5 calculated for the example circuit in Fig. 1. In this case, the current response arising from the augmented matrix can be decomposed in the four dominant contributions illustrated in Fig. 6, leading to:

$$\mathbf{I} = \underbrace{\mathbf{Y}_F\mathbf{V}}_{\mathbf{I}_F} + \underbrace{\mathbf{Y}_{DC}\mathbf{V}}_{\mathbf{I}_{DC}} + \underbrace{\mathbf{Y}_S\mathbf{V}}_{\mathbf{I}_S} + \underbrace{\mathbf{Y}_{LTI}\mathbf{V}}_{\mathbf{I}_{LTI}} \tag{11}$$

where $\mathbf{I} = [I_{-N} \ldots, I_{+N}]^T$ and $\mathbf{V} = [V_{-N}, \ldots, V_N]^T$ collect the harmonics of the steady-state current and voltage responses.

A. Fully coupled behavior ($\mathbf{Y}_F$)

Block $\mathbf{Y}_F$ consists of a null matrix filled-in with a fully coupled central kernel only. It represents a reduced order PLTV approximation of the switching behavior of the converter which is related to its low-frequency functional operation. The effect of such block mainly affects the low-frequency components of the current spectrum (i.e., the first $\tilde{N}$ harmonics, for $\tilde{N} \approx 5 - 20$), but it can be neglected at the high-frequency.

B. DC term ($\mathbf{Y}_{DC}$)

This block consists of a null matrix with the exception of the central row outside the fully coupled block. It provides the dc (i.e., constant) contribution of the absorbed current arising from the coupling between the high-frequency components of the port voltage response and the central column of the augmented admittance matrix,

$$I_{DC} = \sum_{\tilde{N}<|n|\leq N} Y_n(-n\omega_c)V_{-n}. \quad (12)$$

In a vector form the above equation writes:

$$\mathbf{I}_{DC} = [0, \ldots, 0, I_{DC,0}, 0, \ldots, 0]^T, \quad (13)$$

where only the central harmonic $I_{DC,0}$ differs from zero.

C. High-frequency source term ($\mathbf{Y}_S$)

The source term corresponds to the central column of the admittance matrix. It represents the coupling between the dc value of the excitation (hereafter labeled as V_0) and the higher frequency harmonics of the current response:

$$I_{S,n} = \begin{cases} 0, & \text{for } |n| \leq \tilde{N} \\ Y_n(0)V_0, & \text{for } |n| > \tilde{N}. \end{cases} \quad (14)$$

In a vector form, the above contribution writes:

$$\begin{aligned} \mathbf{I}_S &= [I_{S,-N}, \ldots, I_{S,-\tilde{N}-1}, 0, \ldots, 0, I_{S,\tilde{N}+1}, \ldots, I_{S,N}]^T \\ &= V_0[Y_{-N}(0), \ldots, Y_{-\tilde{N}-1}(0), 0, \ldots \\ &\quad \ldots 0, Y_{\tilde{N}+1}(0), \ldots, Y_N(0)]^T. \end{aligned} \quad (15)$$

D. Dominant LTI behavior ($\mathbf{Y}_{LTI}$)

According to [11], [13], the diagonal terms of the admittance matrix represent the LTI admittance behavior of the circuit element. The harmonics of the current response arising from this contribution writes:

$$\begin{aligned} I_{LTI,n} &= Y_0(n\omega_c)V_n \\ &= Y_{LTI,nn}V_n, \quad \text{for } \tilde{N} < |n| \leq N,\ n \in \mathbb{Z}, \end{aligned} \quad (16)$$

where the terms $Y_{LTI,nn}$ are the diagonal elements of $\mathbf{Y}(0)$.

V. Enhanced Norton Model

Based on the previous discussion on the admittance matrix decomposition, this section presents a new enhanced Norton model that can be justified within the robust theoretical framework of PLTV systems.

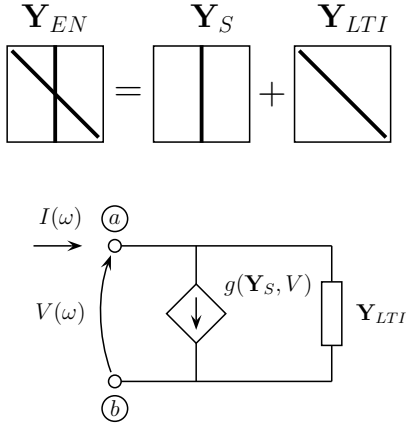

Figure 7: Proposed enhanced Norton-based model.

For the class of switching elements that exhibits a *low-frequency coupling* (i.e., a shape of the admittance matrix similar to the one of Fig. 5), the simplification shown in top panel of Fig. 7 can be adopted. The latter is a simplified representation of the augmented admittance matrix $\mathbf{Y}(\Omega = 0\,\text{rad/s})$ consisting of the diagonal term $\mathbf{Y}_{LTI}$ and of the high-frequency source term $\mathbf{Y}_S$, being the contribution of the fully coupled block $\mathbf{Y}_F$ and of the DC term $\mathbf{Y}_{DC}$ negligible at high-frequency. The above interpretation suggests to represent the frequency-domain i-v characteristic of the input port of the switching element by means of the equivalent circuit shown in the bottom panel of Fig. 7. It is important to remark that such low-frequency coupling behavior is shared by most of the switching devices (e.g., inverters, DC motors, switching converters, etc.). The nature of such low-frequency coupling is related to the fact that the Fourier coefficients describing the time-varying behavior of the switches decrease in frequency as least as $1/f$ [13].

According to Fig. 6, matrix $\mathbf{Y}_S$ can be interpreted as a voltage controlled current source defined in frequency-domain providing the coupling between the DC voltage excitation V_0 and the harmonics of the current response I_n generated by the commutation of switch. From (15), the non-zero elements of $\mathbf{Y}_S$ can be calculated from the absorbed current of the PLTV element recorded at nominal operating condition (e.g., $\Omega = 0\,\text{rad/s}$). In particular, the central column of the matrix is filled in by $(2N+1)$ positive and negative harmonics of the measured current sampled at the integer multiples of the switching angular frequency ω_c and normalized by the value of dc voltage excitation V_0.

On the other hand, the matrix $\mathbf{Y}_{LTI}$ collects the coefficients corresponding to the one-to-one coupling that involves the pairs of the voltage and current harmonics at the same frequency, thus allowing to incorporate the dominant LTI behavior of the switching element. As reported in (16), the latter term is obtained by sampling the spectra of the input port voltage and current responses at integer multiples of the switching angular frequency ω_c and by computing $\mathbf{Y}_{LTI,n}$ as the ration between the n-th current and voltage harmonics.

This alternative yet simplified model structure has two main advantages with respect to the full augmented matrix characterization: (i) it can be estimated from two measurements, only, (i.e., the spectrum of the absorbed current $i(t)$ at the nominal condition and the input admittance $\mathbf{Y}_{LTI}(\omega)$) via the setup in Fig. 4 and (ii) it offers nearly the same accuracy of the full-admittance characterization (e.g., see the results of Sec. VI). Also, the proposed enhanced Norton model can be interpreted as the generalization of classical LTI Norton models for the case of PLTV circuits.

It is worth to remark that the proposed model represents an effective and viable solution for the generation of accurate models from real measured data, and it is valid for the wide class of switching circuits under the assumption that the linear working condition is guaranteed. Indeed, similar to the standard LTI Norton model, the accuracy provided by both the augmented admittance matrix and the enhanced Norton is guaranteed until the switching device works in a linear conditions. This means that even if the proposed models are

expected to have a lower sensitivity to a possible change in the working condition of the device with respect to a plain LTI Norton approximation, a large variation with respect to the nominal supply condition may lead to a possible inaccurate predictions due to the unpredictable contributions of nonlinear effects e.g., core saturation of the inductors or changing in the operation mode. The CE prediction is done via the simulation procedure of Sec. III-C by replacing the full admittance $\mathbf{Y}$ with the enhanced Norton matrix $\mathbf{Y}_{EN}$.

VI. Experimental Results

In this section the feasibility and the robustness of proposed modeling approaches are demonstrated via the prediction of CE generated by a dc-dc boost converter and a dc-motor under different supply configurations. In particular, the predictions of a classical LTI Norton model are compared with the ones provided by the full augmented admittance matrix and the enhanced Norton model.

In both examples, CE are measured by means of the standard setup of Fig. 8, where the device under test (DUT) (e.g., the boost converter or the dc-motor) is connected to the supply main through a possible filter and a line impedance stabilization network (LISN). The differential mode (DM) CE are computed from the output voltages $V_{LG}(\omega)$ and $V_{NG}(\omega)$ of the LISN. It is worth mentioning that a similar procedure can be applied, without any modification, to the prediction of the common mode (CM) emission.

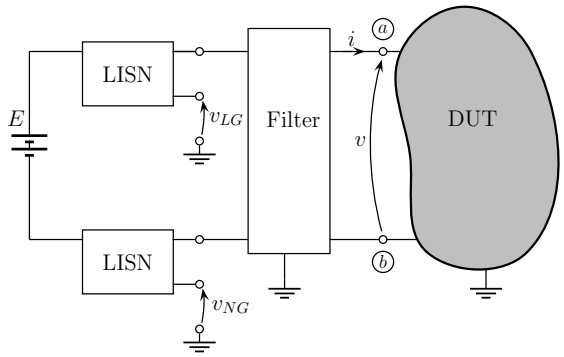

Figure 8: Setup for the measurement of the CE characterization.

A. DC-DC Boost Converter

In this first application example, the proposed full-admittance and enhanced Norton modeling are used to predict the DM CE of the boost converter shown in Fig. 9 for different supply conditions. The converter operates in continuous mode at a switching frequency $f_c = 50\,\text{kHz}$, with duty cycle $D = 50\%$ and a nominal input voltage $v = 5\,\text{V}$. The circuit parameters take the following values: $L = 470\,\mu\text{H}$, $C = 470\,\mu\text{F}$, $R = 150\,\Omega$ with a FES16DT diode and a IRFU4105 n-channel MOS, respectively.

As a first test, the augmented admittance $\mathbf{Y}$ of the converter has been estimated for an expansion order $N = 15$ via the modeling approach proposed in Sec. III-C. A total number of 31 current and voltage measurements are carried out. Figure 11

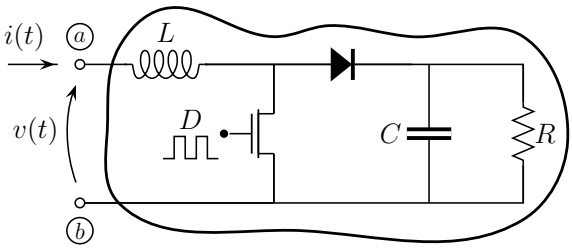

(a)

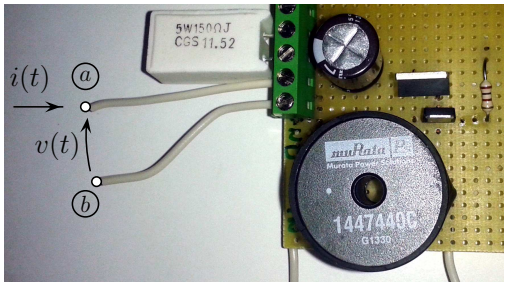

(b)

Figure 9: Schematic (panel (a)) and test-board (panel (b)) of the considered dc-dc boost converter.

compares the admittance matrices estimated from measured data with the one computed via numerical simulations [27]. The above comparison provides a first accuracy check, highlighting the good agreement between the analytical and the measured stamps, thus confirming the effectiveness of the proposed modeling approach.

The set of absorbed currents has been estimated from the voltage drop $v_L(t)$ across the inductor L of the converter, which has been previously characterized in frequency-domain. The measurements are performed in time-domain by means of a digital scope (LeCroy 7300A and passive voltage probes) and the corresponding spectra are computed offline via MATLAB and the discrete time Fourier transform (DTFT) routine. The sinusoidal voltage excitations $e(t)$ are generated by a waveform generator (Agilent 33250A). For all measurements, an observation time of $200\,\mu\text{s}$ corresponding to 10 switching periods with a time step $\Delta_t = 2\,\text{ns}$ is adopted. The measurements sampling is synchronized with the switching signal of the system.

As an example Fig. 10 shows the steady-state responses corresponding to one of the 31 current and voltage measurements used for the estimation of the admittance matrix. This figure compares the measured waveforms with the predictions obtained via the augmented admittance representation of the converter in Fig. 5 and the simulation approach proposed in [13], [16]. The different curves in the figure are the voltage excitation $v(t)$ applied to the input port of the converter consisting of the superposition of a $3\,\text{V}$ dc voltage with a sinusoidal signal of frequency $250\,\text{kHz}$, and the voltage $v_L(t)$ across the inductor which is then used to calculate the absorbed current $i(t)$.

As a second test, the CE of the converter are measured

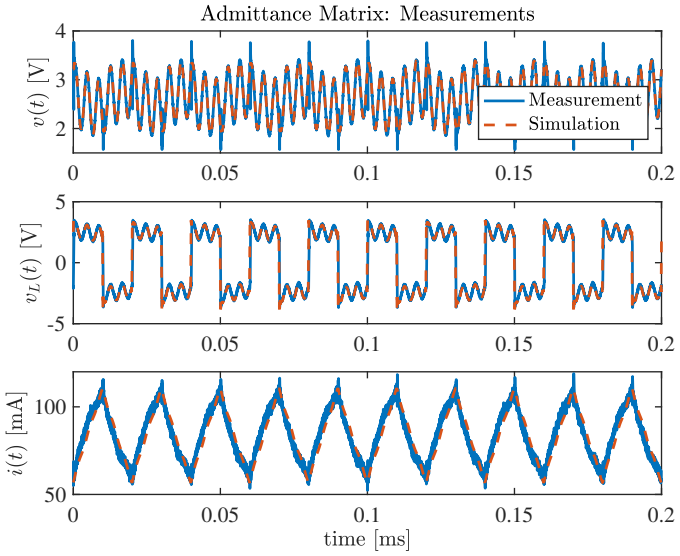

Figure 10: Example voltage and current responses used for the estimation of the full admittance matrix $\mathbf{Y}(\Omega = 0\,\text{rad/s})$ of the boost converter of Fig. 1. Solid blue: measurement; dashed red: simulation results.

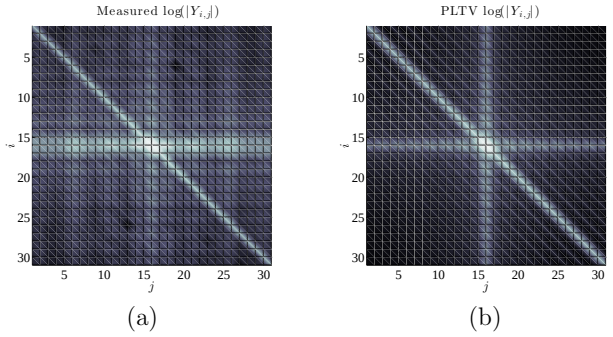

Figure 11: Comparison between the measured (left panel) and the simulated (right panel) admittance matrix $\mathbf{Y}$ for $N = 15$ of the boost converter of Fig. 1. The grayscale image provides a graphical information of the absolute values of the matrix entries; the white color corresponds to the highest magnitudes.

via the setup of Fig. 8 when a resistor $R_s = 56\,\Omega$ is inserted between the LISN and the converter with the aims of stressing the capability of the proposed frequency-domain approaches in predicting the CE for different supply configurations.

Figure 12 compares the measured CE spectrum with the one predicted by the full-admittance, the enhanced Norton and the standard LTI Norton modeling techniques. All the models are obtained at the standard supply condition $E = 5\,\text{V}$. The curves of Fig. 12 highlight the improved accuracy of the proposed enhanced Norton model and augmented full-admittance matrix representations with respect to the plain LTI Norton model. Also, as briefly outlined in the last sentence of Sec. III-C, the dashed-black curve in the bottom panel of the Figure confirms that the full-admittance matrix obtained for $N = 31$ does not allow to completely characterize the frequency bandwidth 150 kHz–30 MHz required for the CE. In fact, the bandwidth covered by the above model is not enough to predict the sharp peaks in the time waveforms, being the latter associated to the high-frequency portion of the spectrum, which is not accounted for in the full-admittance matrix [14] (i.e., the maximum frequency covered by the full-admittance model is $f_{max} = N \cdot f_c = 750\,\text{kHz}$ as shown in the spectrum of Fig. 12 (bottom panel)).

Indeed, for the test case of Fig. 8 and the required bandwidth $f_{max} = 30\,\text{MHz}$, the expansion order $N = f_{max}/f_c$ required to cover the whole bandwidth turns out to be greater than 600, thus making the direct application of the procedure of Sec. III-C inefficient and in part unfeasible for a complete CE characterization. On the other hand, the enhanced Norton model provides nearly the same results of the full-admittance case for the low-frequency region and extends its validity for larger frequencies, thus justifying the remarkably good features of the proposed simplified approach.

It is ought to remark that the augmented admittance matrix and the enhanced Norton modeling techniques considered in this section can be considered as an extension of the well-known concept of equivalent impedance or admittance used for the LTI circuits to the case of linear time-varying ones. Therefore they turn out to be independent from the instruments used to drive the device under test and by the approach used to measure input port voltage and current waveforms.

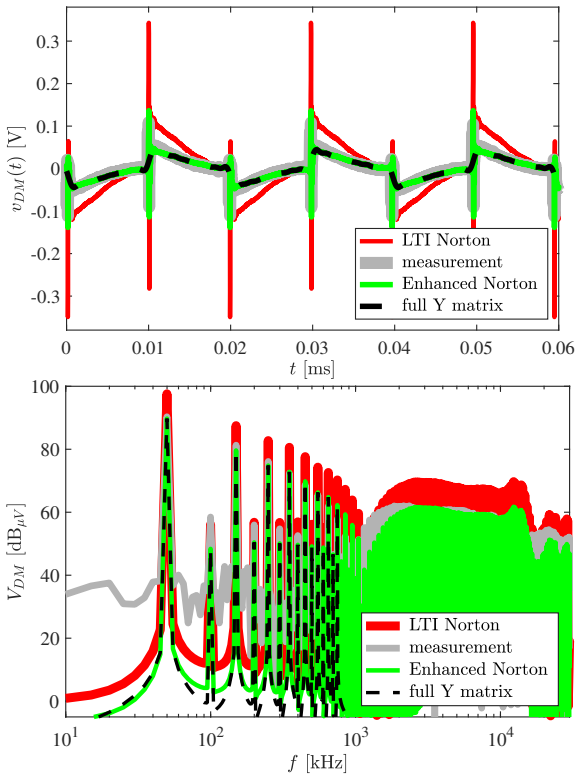

Figure 12: Measured and predicted noisy spectra V_{DM} generated by the boost converter in Fig. 1 with a resistor of $R_s = 56\,\Omega$. Solid light grey: measurement; solid red: LTI Norton-based prediction; solid green: proposed enhanced Norton-based method; dashed black: full-admittance matrix characterization.

B. DC-motor

To further stress the generality of the proposed modeling approach, a second yet relevant application involving the commercial electrical motor shown in Fig. 13 is presented. The motor is a 12 windings dc motor with brushes working at the nominal voltage of 12 V, with a rotation speed of 3585 rpm.

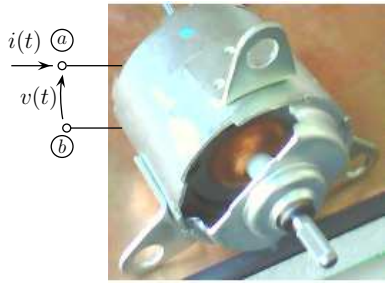

Figure 13: Brushes DC-motor.

As already done for the boost converter, the DM CE of the motor are measured via the measurement setup in Fig. 8 for different values of the supply main V_{DC} and with and without a capacitive EMI mitigation filter consisting of two 474 nF capacitors connected between the (a)-(b) terminals of the motor and the the reference ground. In this example, the switching frequency f_c is inherently defined by the rotation speed of the motor and takes the value $f_c = 3585/60$ Hz, for $E = 12$ V, leading to $N > 10,000$ for the required bandwidth $f_{max} = 30$ MHz. Again, the direct application of the procedure in Sec. III-C involves a large number of measurements, thus making the enhanced Norton approach more desirable.

The impedance and the voltage controlled current source of the enhanced Norton have been defined according to the average input impedance shown in Fig. 14 and from the differential mode current $I(\omega)$ absorbed by the motor at the nominal operating condition with $V_{in} = 12$ V without the capacitive filter. All the measurements are performed by means of a digital oscilloscope (LeCroy 7300A and passive voltage probes) by considering an observation time of 5 ms and a fixed time step of 4 ns.

Figure 15 compares the measured spectra of the DM emissions with the predictions obtained by the standard LTI Norton and the enhanced Norton models. The accuracy of the two models is investigated by considering three different configurations of the measurement setup, specifically:

- $E = 12$ V with the capacitive filter (top panel);
- $E = 10$ V without the capacitive filter (central panel);
- $E = 10$ V with the capacitive filter (bottom panel).

According to the results in Fig. 15, when the motor operates at its nominal voltage $E = 12$ V (i.e., the working condition used to build the propose models), the accuracy of the plain LTI Norton model turns out to be equivalent to the one obtained by the proposed enhanced Norton model. On the other hand, when the supply condition is changed to $E = 10$ V, the results confirm the superior accuracy of the proposed enhanced Norton with respect to the plain Norton model, a similar behavior can be seen also when a component is

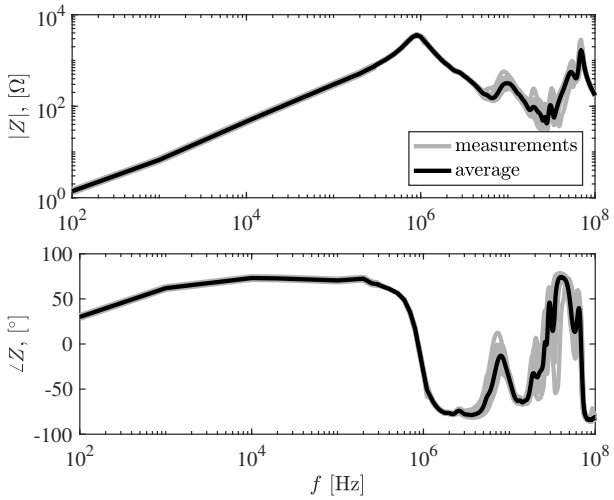

Figure 14: Magnitude and phase of the input impedance $Z_N(\omega)$ of the example dc-motor for 12 different static positions of the rotor (solid gay curves) and the corresponding average values computed from the available measurements (solid black curve).

connected in series at the input port of the switching device. It is important to remark that a possible different speed of the motor can be readily included into the proposed model by simply changing the angular frequency $\omega_c = 2\pi f_c$ in the Fourier expansion of (4), e.g., $f_c = 2500/60$Hz for $V_{in} = 10$ V).

VII. Conclusions

In this papers, an alternative modeling approach for the prediction of the conducted emissions of switching devices is presented. The main contribution of the research study carried out is twofold. On one side, a robust and general modeling framework is developed where the theory of periodical switched linear systems is used to generate an augmented device port characterization of a switching circuit. The parameters of the above representation are computed from real measurements and the solution of a linear problem. On the other hand, a more practical solution based on an enhanced Norton-like model is formally derived. In the latter case, the modeling scheme is simplified. This simplification still enables the application of the method to a wide class of examples and devices including switching power converters and dc electrical motors. The proposed approach is compared with the classical state-of-the-art standard techniques based on the generation of linear time invariant equivalents, thus highlighting its superior modeling accuracy. Two application test cases (a dc boost converter and a dc electrical motor) are thoroughly discussed and the CE predictions are compared with real measurements.

References

[1] V. Tarateeraseth, S. Kye Yak, F.G. Canavero, R.W. Chang, "Systematic Electromagnetic Interference Filter Design Based on Information From In-Circuit Impedance Measurements", *IEEE Trans. on Electromagn. Compat.*, vol. 52, no. 3, pp. 588–598, Aug. 2010.

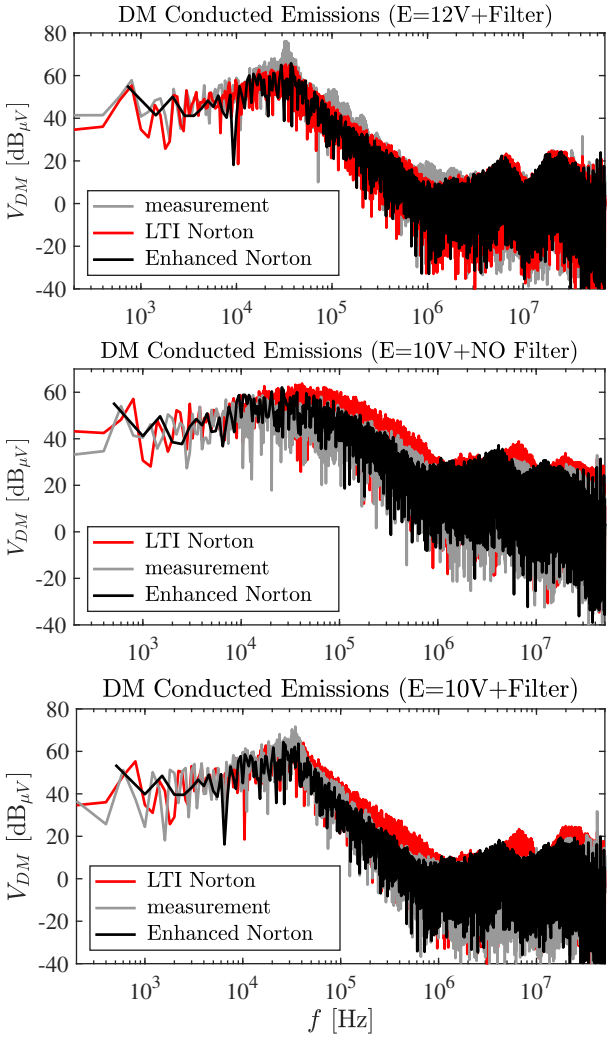

Figure 15: DM noise voltage response of the validation test case shown in Fig. 8 with the dc motor of Fig. 13 for different supply configurations (see text for details). Solid light gray: measurement; Solid red: LTI Norton-based prediction; solid black: proposed enhanced Norton-based method.

[2] X. Pei, Jian Xiong, Y. Kang, J. Chen, "Analysis and suppression of conducted EMI emission in PWM inverter", in Proc. of the *Int. Conf. IEMDC'03 on Electric Machines and Drives*, Vol. 3, pp. 1787–1792, June 2003.

[3] Y. Koyama, M. Tanaka, H. Akagi,"Modeling and analysis for simulation of common-mode noises produced by an inverter-driven air conditioner", in Proc. of *Int. Conf. on Power Electronics (IPEC)*, pp. 2877–2883, June 2010.

[4] E. Rondon-Pinilla, F. Morel, C. Vollaire, J.-L. Schanen, "Modeling of a Buck Converter With a SiC JFET to Predict EMC Conducted Emissions", *IEEE Trans. on Power Electronics*, vol. 29, no. 5, pp. 2246–2260, May 2014.

[5] J. Benecke, "Impedance and Emission Optimization of Low-Voltage DC Motors for EMC Compliance," *IEEE Trans. on Industrial Electronics*, vol. 58, no. 9, pp. 3833–3839, Sept. 2011.

[6] L. A. Zadeh, "Frequency Analysis of Variable Networks", *Proceedings of the IRE*, vol. 38, no. 3, pp. 291–299, Mar. 1950.

[7] T. Strom, S. Signell, "Analysis of periodically switched linear circuits", *IEEE Trans. Circuits and Systems*, vol. 24, no. 10, pp. 531–541, Oct. 1977.

[8] T. A. C. M. Claasen, W. F. G. Mecklenbrauker, "On stationary linear time-varying systems", *IEEE Tran. on Circuits and Systems*, vol. 29, no. 3, pp. 169–184, Mar. 1982.

[9] H. Behjati, L. Niu, A. Davoudi, P. L. Chapman, "Alternative Time-Invariant Multi-Frequency Modeling of PWM DC-DC Converters", *IEEE Trans. on Circuits and Systems I: Regular Papers*, vol. 60, no. 11, pp. 3069-3079, Nov. 2013.

[10] H. Sandberg, E. Mollerstedt, Bernhardsson, "Frequency-domain analysis of linear time-periodic systems", *IEEE Trans. on Automatic Control*, vol. 50, no. 12, pp. 1971–1983, Dec. 2005.

[11] J. Roychowdhury, "Reduced-order modeling of time-varying systems", *IEEE Transactions on Circuits and Systems II: Analog and Digital Signal Processing*, vol. 46, no. 10, pp. 1273–1288, Oct 1999.

[12] R. Trinchero, I. S. Stievano, F. G. Canavero, "Steady-State Response of Periodically Switched Linear Circuits via Augmented Time-Invariant Nodal Analysis", *Journal of Electrical and Computer Engineering*, vol. 14, no. 4, pp. 3-8, 2014.

[13] R. Trinchero, I. S. Stievano, F. G. Canavero, "Steady-State Analysis of Switching Power Converters Via Augmented Time-Invariant Equivalents", *IEEE Trans. on Power Electronics*, vol. 29, no. 11, pp. 5657–5661, Nov. 2014.

[14] R. Trinchero, I. S. Stievano, F. G. Canavero, "EMI Prediction of Switching Converters," *IEEE Trans. on Electromagnetic Compatibility*, vol. 57, no. 5, pp. 1270–1273, 2015.

[15] R. Trinchero, I. S. Stievano, "F-Domain Analysis of Linear Circuits with Time-Varying Parameters via Integral Equations," in Proc of the *IEEE International Symposium on Circuits and Systems (ISCAS)*, Florence, 2018, pp. 1-5.

[16] R. Trinchero, P. Manfredi, I. Stievano, F. Canavero, "Steady-State Analysis of Switching Converters via Frequency-Domain Circuit Equivalents," *IEEE Trans. on Circuits and Systems II: Express Briefs*, vol. 63, no. 8, pp. 748–752, Aug. 2016.

[17] F. Bizzarri, A. Brambilla and G. Storti Gajani, "Steady State Computation and Noise Analysis of Analog Mixed Signal Circuits," *IEEE Trans. on Circuits and Systems I: Regular Papers*, vol. 59, no. 3, pp. 541-554, March 2012.

[18] M. Nakhla, J. Vlach, "A piecewise harmonic balance technique for determination of periodic response of nonlinear systems," *IEEE Trans. Circuits and Systems*, vol. 23, no. 2, pp. 85–91, Feb 1976.

[19] V. Tarateeraseth, I.A. Maio, F.G. Canavero, "Assessment of Equivalent Noise Source Approach for EMI Simulations of Boost Converter", in Proc. of the *20th Int. Zurich Symposium on EMC*, pp. 353–356, Jan. 2009.

[20] Y. Liu, Kye Yak See, King-Jet Tseng, "Conducted EMI Prediction of the PFC Converter Including Nonlinear Behavior of Boost Inductor", *IEEE Trans. on Electromagn. Compat.*, vol. 55, no. 6, pp. 1107–1114, Dec. 2013.

[21] F. Yang, X. Ruan, Q. Ji, Z. Ye, "Input Differential-Mode EMI of CRM Boost PFC Converter", *IEEE Trans. on Power Electronics*, vol. 28, no. 3, pp. 1177–1188, March 2013.

[22] R. Kahoul, Y. Azzouz, P. Marchal, B. Mazari, "New Behavioral Modeling for DC Motor Armatures Applied to Automotive EMC Characterization", *IEEE Trans. on Electromagn. Compat.*, vol. 52, no. 4, pp. 888–901, Nov. 2010.

[23] R Kahoul, Y. Azzouz, B. Ravelo, B. Mazari, "New Behavioral Modeling of EMI for DC Motors Applied to EMC Characterization," *IEEE Trans. on Industrial Electronics*, Vol. 60, no. 12, pp. 5482–5496, Dec. 2013.

[24] F. Diouf, F. Leferink, F. Duval, M. Bensetti, "Wideband Impedance Measurements and Modeling of DC Motors for EMI Predictions," *IEEE Trans. on Electromagn. Compat.*, vol. 57, no. 2, pp. 180–187, April 2015.

[25] Jian Sun, Lei Xing, "Parameterization of Three-Phase Electric Machine Models for EMI Simulation", *IEEE Trans. on Power Electronics*, vol.29, no. 1, pp. 36–41, Jan. 2014.

[26] H. Bishnoi, P. Mattavelli, R. Burgos, D. Boroyevich, "EMI Behavioral Models of DC-Fed Three-Phase Motor Drive Systems", *IEEE Trans. on Power Electronics*, vol. 29, No. 9, pp. 4633–4645, Sept. 2014.

[27] R. Trinchero, I. S. Stievano, F. G. Canavero, "EMI modeling of switching circuits via augmented equivalents and measured data," in Proc. of the *IEEE International Symposium on Electromagnetic Compatibility (EMC)*, Dresden, 2015, pp. 130–133.

[28] M. Nakhla, J. Vlach, "A piecewise harmonic balance technique for determination of periodic response of nonlinear systems," *IEEE Trans. on Circuits and Systems*, vol. 23, no. 2, pp. 85–91, February 1976.

Riccardo Trinchero (M'16) was born in Casale Monferrato, Italy in 1987. He received the M.Sc. and the Ph.D. degrees in Electronics and Communication Engineering from Politecnico di Torino, Torino, Italy, in 2011 and 2015, respectively.

He is currently a Researcher within the EMC Group with the Department of Electronics and Telecommunications at the Politecnico di Torino. His research interests include the analysis of linear time-varying systems, modeling and simulation of switching converters and statistical simulation of circuits and systems.

Igor S. Stievano (M'98–SM'08) received the Master?s degree in electronic engineering and the Ph.D. degree in electronics and communication engineering from the Politecnico di Torino, Turin, Italy, in 1996 and 2001, respectively. He is currently a Professor of electrical engineering with the Department of Electronics and Telecommunications, Politecnico di Torino. He has authored or coauthored more than 130 papers published in international journals and conference proceedings. His current research interests include electromagnetic compatibility and signal integrity, with emphasis on modeling and simulation of digital circuits, transmission lines, PLC channels, switching converters, development of stochastic methods for the statistical simulation of circuits and systems, and the compact modeling of electrical and gas networks via a complex network paradigm and simplified graph-based approaches. He was the Program Co-Chair of the 20th and 21st IEEE Workshops on Signal and Power Integrity (SPI2016 and SPI2017). Since 2017, he has been the Vice Rector on Academic and Scientific activities of the joint campus of the Politecnico di Torino, in Uzbekistan, Turin Polytechnic University in Tashkent (TTPU).

Flavio G. Canavero (SM'99-F'07) received his electronic engineering degree from Politecnico (Technical University) of Torino, Italy, and the PhD degree from the Georgia Institute of Technology, Atlanta, USA, in 1986. Currently he is a Professor of Circuit Theory with the Department of Electronics and Telecommunications, Politecnico di Torino. He is an IEEE Fellow. He has been the Editor-in-Chief of IEEE Transactions on Electromagnetic Compatibility, V.P. for Communication Services of the EMC Society and Chair of URSI Commission E. He received several Industry and IEEE Awards, including the prestigious Richard R. Stoddard Award for Outstanding Performance, which is the EMC Society's highest technical award, and the Honored Member Award of EMC Society. His research interests include signal integrity and EMC design issues, interconnect modeling, black-box characterization of digital integrated circuits, EMI and statistics in EMC.